Numerical Comparison of Triangular and Sinusoidal External Vibration Effects on the 3D Porous Drying Process

Nidhal Ben Khedher
Mechanical Engineering Department
University of Hail
Hail, Saudi Arabia and
National School of Engineers of
Monastir, University of Monastir
Monastir, Tunisia

Rzig Ramzi
Thermal and Energy Systems Studies
Laboratory
National School of Engineers of
Monastir
University of Monastir
Monastir, Tunisia

Ibrahim A. Alatawi
Mechanical Engineering Department
College of Engineering
University of Hail
Hail, Saudi Arabia

***Abstract*—Drying is one of the most energy-intensive industrial processes. One of the techniques aiming to reduce energy consumption is the vibration technique which is generally employed to intensify the heat and mass transfer process. In this respect, this paper presents a three-dimensional numerical model to study the external vibration effects on the drying process of a porous medium. The model is based on a comparison of heat and mass transfer phenomena that arise during vibrating drying of unsaturated porous medium for two cases: triangular and sinusoidal external vibrations. The three-dimensional unstructured Control Volume Finite Element Method (CVFEM) is employed to simulate the vibrating drying. Numerical results of the time evolution of temperature, liquid saturation, pressure, and water content are compared and analyzed for the two cases.**

Keywords-external vibration; vibrating drying; unsaturated porous medium; CVFEM

I. INTRODUCTION

The problem of intensification of heat and mass transfer in porous media has attracted considerable attention over the last years. This interest has been motivated by a large domain of industrial applications, including food, wood, paper, building, ceramic, etc. To solve this problem, more efficient technologies have been employed. The development of the vibration phenomenon in porous media has been an emerging subject in many fields of science and engineering. The vibration phenomenon has been found to enhance heat and mass transfer process and to improve systems efficiency. For many years research has been interested in heat and mass transfer during the drying process which is one of the oldest processes in porous media, characterized by coupled heat and mass transfer phenomena. However, the consumption of high quantity of energy during porous solids drying has made it an interesting subject in scientific and technological range with a variety of industrial applications. Also, high cost and long execution time of experimental studies made the numerical simulation widely employed to analyze the drying process. In consequence, research focuses on the employment of more efficient technologies to intensify the drying process [1].

Recently, several methods have been developed as the technique of drying with ultrasonic [2] and later with acoustic [3] frequencies. These two techniques present many disadvantages such as high noise level and low energy efficiency. Consequently, the vibration is an important alternative gaining increasing [4]. Authors in [5] investigated the influence of airborne ultrasound conditions on drying. Moreover, authors in [6] studied the drying intensification by vibration. Also, authors in [7] studied the vibration effect on convection excitation in fluid and porous layers. Recently, authors in [8] conducted a numerical analysis of the effect of vertical vibrations on heat and mass transfer through natural convection in a partially porous cavity. More recently, authors in [9] developed a 3-D numerical model to study the vibration effects on the drying process. The motivation of this study is that the vibration is a new technology for the amelioration of drying process which deserves to be further studied and analyzed.

The aim of the present paper is to offer a numerical study that can explain the external vibration effects on the drying process through a comparison between two configurations of vibration (triangular and sinusoidal vibrations). In this context, a 3-D numerical model is employed to describe the coupled heat and mass transfer phenomena during vibrating drying of unsaturated porous plate. The numerical results of studying the effects of the two types of vibration on the drying process are presented and analyzed.

II. GOVERNING EQUATIONS

The proposed model is based on a numerical problem treating a comparison of external vibration effects of hot air on heat and mass transfer during the drying of unsaturated porous medium. The physical domain is a porous plate composed of three phases (solid, liquid and gas). The geometry of the plate can be seen in Figure 1.

Corresponding author: Nidhal Ben Khedher (n.khedher@uoh.edu.sa)

Fig. 1. Dimensions and geometry of the porous plate

The numerical model is a comparison of heat and mass transfer during the drying process for three configurations of drying (hot air velocity):

- Classical drying (without vibration):

$$V_a = 10\,\mathrm{m/s} \quad (1)$$

- With triangular vibration:

$$V_a = a \times t + b \quad (\mathrm{m/s}) \quad (2)$$

with:

$$a = \frac{3 \times A_v}{T_v}, b = 0; 0 \le t \le \frac{T_v}{3}$$

$$a = \frac{-6 \times A_v}{T_v}, b = 3 \times A_v; \frac{T_v}{3} \le t \le \frac{2 \times T_v}{3}$$

$$a = \frac{3 \times A_v}{T_v}, b = -3 \times A_v; \frac{2 \times T_v}{3} \le t \le T_v$$

- With sinusoidal vibration:

$$V_a = A_v \times \sin(2 \times \pi \times f_v \times t)(m/s) \quad (3)$$

where $A_v\,(A_v = 10\,\mathrm{m/s})$ is the maximum amplitude of vibrating velocity, t is the time, $T_v\,(T_v = 0.2\mathrm{s})$ and $f_v\,(f_v = 5\mathrm{Hz})$ are respectively the period and the frequency of vibrating velocity and a is the acceleration. The periodic evolution of hot air velocity for the two configurations of vibrating drying (triangular and sinusoidal) are presented in Figure 2.

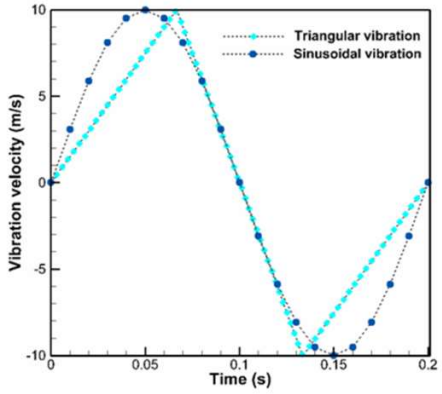

Fig. 2. Evolution of hot air velocity during a period for triangular and sinusoidal vibrations

Referring to the theory given in [10-12], various mathematical versions have been employed to describe the drying phenomenon for porous media.

A. Thermodynamic Relations

The partial pressure of the vapor is equal to its equilibrium pressure:

$$P_v = P_{veq}(T, S) \quad (4)$$

where S is the liquid saturation defined by:

$$S = \frac{\varepsilon_l}{\varepsilon} \quad (5)$$

The gaseous phase is assumed to be an ideal mixture of perfect gases:

$$\overline{P_i} = \frac{\overline{\rho_i}}{M_i} R\overline{T}; i = a \quad (6)$$

$$\overline{P_g} = \overline{P_a} + \overline{P_v}$$

$$\overline{\rho_g} = \overline{\rho_a} + \overline{\rho_v}$$

The vapor pressure is given by:

$$\frac{P_v}{P_{vs}} = exp\,(-\frac{2.\sigma.M_v}{r.\rho_l.R.T}) \quad (7)$$

The presented model has the following assumptions:

- The porous plate is homogenous and isotropic.
- The three phases (solid, liquid, and gas) are in local thermodynamic equilibrium.
- The gaseous phase is thermodynamically ideal.
- The terms of tortuosity and dispersion are considered as diffusion terms.
- The work of compression and the viscous dissipation are negligible.
- The radiative heat transfer is negligible.

Based on the above assumptions, the macroscopic equations for the heat and mass transfer that arise during the drying of porous medium can be derived.

B. Generalized Darcy's Law

The average velocities of gaseous and liquid phases, which are noted respectively as $\overline{V_g}$ and $\overline{V_l}$, are obtained from Darcy's Law which is generalized by using the relative permeability (calculated as the ratio between the intrinsic permeability and the effective permeability).

- The gaseous phase:

$$\overline{V_g} = -\frac{KK_g}{\mu_g} \nabla \overline{P_g}^{\,g} \quad (8)$$

The gaseous velocity is calculated without taking into consideration the gravitational effect.

- The liquid phase:

$$\overline{V_l} = -\frac{KK_l}{\mu_l}\left[\nabla\left(\overline{P_g}^{\,g} - P_c\right) - \overline{\rho_l}^{\,l} g\right] \quad (9)$$

where $P_c = \overline{P_g}^{\,g} - \overline{P_l}^{\,l}$ is the capillary pressure.

C. Mass Conservation Equations

- The gaseous phase:

For this phase the average density is not constant. In this case, the mass conservation equation is given by:

$$\frac{d\overline{\rho_g}}{dt} + \nabla\left(\overline{\rho_g}^{\,g}\overline{V_g}\right) = \dot{m}_g \quad (10)$$

where $\overline{\rho_g}^{\,g}$ is the intrinsic average density of the gas phase which is considered as an ideal mixture of perfect gases.

- The vapor phase:

$$\frac{d\overline{\rho_v}}{dt} + \nabla\left(\overline{\rho_v}^{\,g}\overline{V_v}\right) = \dot{m}_v \quad (11)$$

$$\overline{\rho_v}^{\,g}\overline{V_v} = \overline{\rho_v}^{\,g}\overline{V_g} - \overline{\rho_g}^{\,g} D_{eff}\nabla\left(\frac{\overline{\rho_v}}{\overline{\rho_g}^{\,g}}\right) \quad (12)$$

D_{eff} represents the coefficient of the effective diffusion of the vapor in the porous medium. This coefficient takes into account the resistance to the diffusion due to tortuosity and the effects of constriction.

- The liquid phase:

Assuming that liquid density is constant, the mass conservation equation of the liquid phase is:

$$\frac{d\varepsilon_l}{dt} + \nabla\left(\overline{V_l}\right) = -\frac{\dot{m}}{\overline{\rho_l}} \quad (13)$$

where $\dot{m}$ is the mass rate of evaporation which is the volume fraction of liquid phase.

D. Energy Conservation Equation

$$\frac{d}{dt}\left(\overline{\rho C_p}\overline{T}\right) + div\left[\left(\overline{\rho_l}^{\,l} C_{pl}\overline{V_l} + \sum_{k=a,v}\overline{\rho_k}^{\,g} C_{pk}\overline{V_k}\right)\overline{T}\right] = \nabla\left(\lambda_{eff}.\nabla\overline{T}\right) - \Delta H_{vap}.\dot{m}_v \quad (14)$$

where ΔH_{vap} is the latent heat of vaporization at temperature $T(K)$, λ_{eff} and $\overline{\rho C_p}$ are respectively the effective thermal conductivity and the constant pressure heat capacity of the porous medium and $\overline{\rho C_p}$ is given by:

$$\overline{\rho C_p} = \overline{\rho_s} C_{ps} + \overline{\rho_l} C_{pl} + \overline{\rho_a} C_{pa} + \overline{\rho_v} C_{pv} \quad (15)$$

where $\overline{\rho_s} C_{ps}$, $\overline{\rho_l} C_{pl}$, $\overline{\rho_v} C_{pv}$ and $\overline{\rho_a} C_{pa}$ are the mass heat capacities of the plate solid matrix, liquid, vapor, and air.

III. Solution Procedure

CVFEM has been widely employed to simulate heat and mass transfer in porous media [13, 14]. Consequently, this method is employed to solve the equation set with boundary conditions [15, 16].

A. Creation of 3-D Meshing

The free mesh generator Gmsh [17] is employed to create the 3-D meshing of the porous plate (Figure 3). Afterwards a Fortran code is developed to describe the coupled heat and mass transfer phenomena that arise during vibrating drying of porous plate.

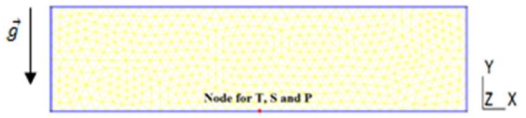

Fig. 3. Three-dimensional porous plate meshing

IV. Boundary Conditions

The variables (temperature, saturation and pressure) are initially uniform in the porous plate (Figure 4).

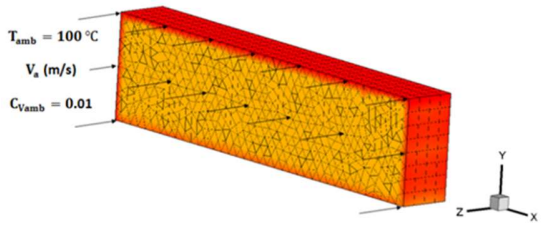

Fig. 4. Drying conditions

On the exchanging faces (right, left, top, front and back faces), we can write:

$$\left[\lambda_{eff}\frac{d\langle T\rangle}{dX_i} + \Delta H_{vap}\rho_l\langle V_l\rangle n_i\right] = h_t(\langle T\rangle - T_\infty) \quad (16)$$

The mass flow corresponding to evaporation and to the evacuation of water is a function of the vapor density difference and mass transfer coefficient:

$$[\rho_l\langle V_l\rangle + \langle\rho_v\rangle^g\langle V_v\rangle]n_i = h_m(C_{vs} - C_{v\infty}) \quad (17)$$

The gaseous pressure on the exchanging face is equal to the atmospheric pressure:

$$\left[\langle P_g\rangle^g\right] = P_{atm} \quad (18)$$

Since the plate is placed on the swing of the dryer, the bottom face does not exchange heat with the hot air. Then, we assume that the bottom face (y=0) is adiabatic and impermeable.

$$\left[\lambda_{eff}\frac{d\langle T\rangle}{dX_i} + \Delta H_{vap}\rho_l\langle V_l\rangle n_i\right] = 0 \quad (19)$$

$$[\rho_l\langle V_l\rangle + \langle\rho_v\rangle^g\langle V_v\rangle]n_i = 0 \quad (20)$$

$$\left[\frac{d\langle P_g\rangle^g}{dX_i}\right] = 0 \quad (21)$$

The convective mass and heat transfer coefficients are given by the following equations [18]. The convective mass transfer coefficient [m/s]:

$$h_m = \frac{D_{A,B}\times 0.023\times R_e^{4/5}\times S_c^{1/3}}{L_c} \quad (22)$$

The convective heat transfer coefficient [w/m^2°C]:

$$h_t = \frac{\lambda \times 0.023 \times R_e^{4/5} \times P_r^{1/3}}{L_c} \quad (23)$$

The validity of these equations is:

$$R_e \prec 5 \times 10^5$$

$$P_r \geq 0.6$$

$$S_c \geq 0.6$$

With:

$$R_e = \frac{\rho_a V_a L_c}{\mu_a}$$

$$P_r = \frac{C_a \mu_a}{\lambda_a}$$

$$S_c = \frac{\vartheta_a}{D_{A,B}}$$

where L_c=0.02m is the characteristic length of porous plate and $D_{A,B}$ is the vapor diffusion in air obtained by:

$$D_{A,B} = D_{vap,air} = 0.26 \times 10^{-4} \left[m^2 s^{-1} \right] \quad (24)$$

The numerical code is validated in [9, 13].

V. NUMERICAL RESULTS AND DISCUSSION

In this section, a 3-D numerical model is employed to study the effects of externals vibrations (triangular and sinusoidal vibrations) on coupled heat and mass transfer during the drying of unsaturated porous plate. The purpose of this study is to analyze the simulation results illustrating the 3-D coupled mechanisms that take place during the vibrating drying. The results are presented for three different configurations of drying:

- Classical drying (without vibration)
- Triangular vibrating drying
- Sinusoidal vibrating drying

For the three cases, the three drying conventional phases are noticed (Figures 5-7):

- The transient heating phase: this phase is characterized by the evolution of the temperature of the material to the wet bulb temperature accompanied by the evaporation a short period in time. Also, a slight depression takes place in this first period.
- The constant drying rate phase: all the heat supplied to the plate is consumed by the evaporation of water to the solid surface whose temperature is evolving to the wet bulb, it homogenizes and remains constant. Moreover, the gas depression reduces without canceling.
- The decreasing drying rate phase (first and second periods): this time period is characterized by evaporation inside the environment and diffusion to the surface. Also, the air diffuses towards the inside.

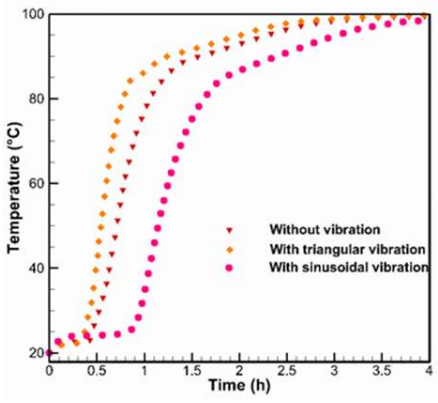

Fig. 5. Comparison of the evolution of temperature

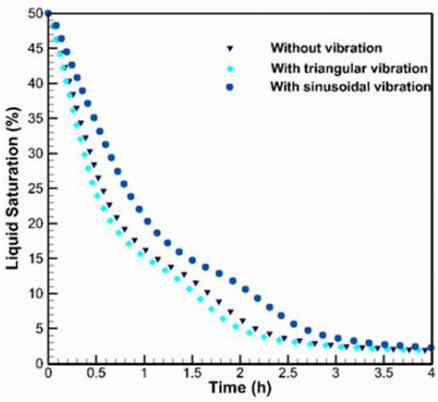

Fig. 6. Comparison of the evolution of liquid saturation

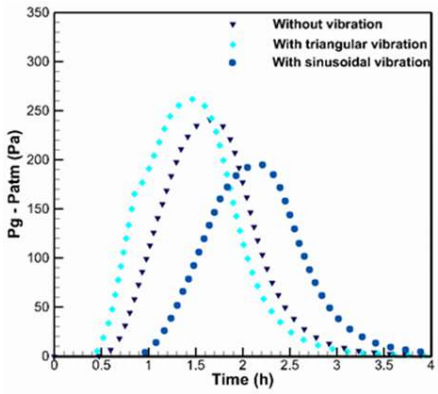

Fig. 7. Comparison of the evolution of pressure

The drying conditions for simulation are presented in Table I.

TABLE I. SIMULATION DRYING CONDITIONS

T_{amb} [°C]	T_{ini} [°C]	S_{ini} [%]	C_{Vamb}	P_{amb} [atm]	P_{ini} [atm]
100	20	50	0.01	1	1

In Figures 5-7, we see a comparison of the time evolution of temperature, saturation and pressure between the three configurations of drying. In Figure 5, it is observed that the profile of temperature for the triangular vibrating drying is more rapid than for the two other drying configurations. Consequently, this configuration implies a rapid drying time. Moreover, the isenthalpic phase (second phase of drying) is clearly longer for the sinusoidal vibrating drying. This delay in time is explained by the fact that the heat and mass transfer coefficients take more time to reach their maximum compared to the triangular vibration. Here, we can conclude that not all air vibration types will surely improve the drying process, but the vibration type should be carefully chosen. Moreover, the vibration period is an important parameter which should be optimized. In this context, the influence of this parameter was detailed in [9]. Figure 6 exhibits a comparison of the time evolution of liquid saturation. From this Figure, it is clearly noted that the triangular vibrating drying presents a gain of time since the liquid saturation drops more rapidly than the other configurations. This gain in time is due to the presence of the triangular vibration which encourages the heat and mass transfer by forcing the liquid inside the plate to move to the exchanging faces, and consequently to be dried more rapidly. Figure 7 depicts the evolution in time of the gaseous pressure for the three configurations of drying (classic, triangular and sinusoidal vibrations). From this figure, it can be noted that the pressure profiles have three different peaks with the more rapid and intense peak corresponding to the triangular vibrating drying while the sinusoidal vibration has the slowest and the weakest gaseous pressure. This behavior is justified by the reasons above which are the time evolutions of heat and mass transfer coefficients which are slower compared to the triangular one.

To be really sure of which vibration type is better, the comparison of time evolution of water content is presented in Figure 8. As expected, the triangular vibration performs better. The triangular vibration forces all the liquid in the porous plate to migrate to the exchanging faces. Consequently, it encourages the evaporation and the diffusion to the surface. In this context, this type of drying encourages the coupled heat and mass transfer to be more intense and rapid, implying a rapid and intense drying.

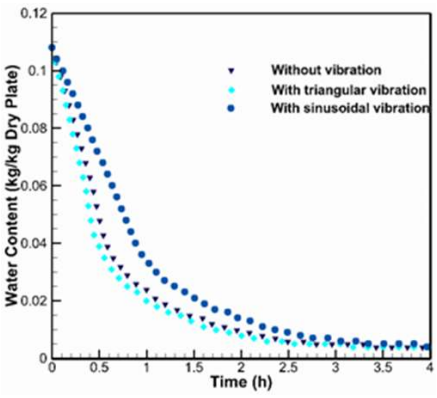

Fig. 8. Comparison of the evolution of water content

To explain more the three dimensional effects of the two configurations of external vibration, it is interesting to exhibit the spatiotemporal evolutions of temperature, saturation and pressure during the drying process. In order to better represent the spatial distribution of different variables for the three cases, the slices view after two hours of drying of temperature, saturation and pressure are shown in Figures 9-11. Figure 9 depicts a 3-D comparison of the temperature distribution along the drying process. Referring to this Figure, and compared to the two other cases, the triangular vibrating drying is the most intense. However, the energy is driven within the plate due to the heat conduction and the presence of the triangular vibration forces the liquid water to be evaporated at the surface of the medium and the moisture moves out of the board dues to the diffusion. Moreover, the sinusoidal vibrating drying presents the lowest evolution of temperature in the whole porous plate.

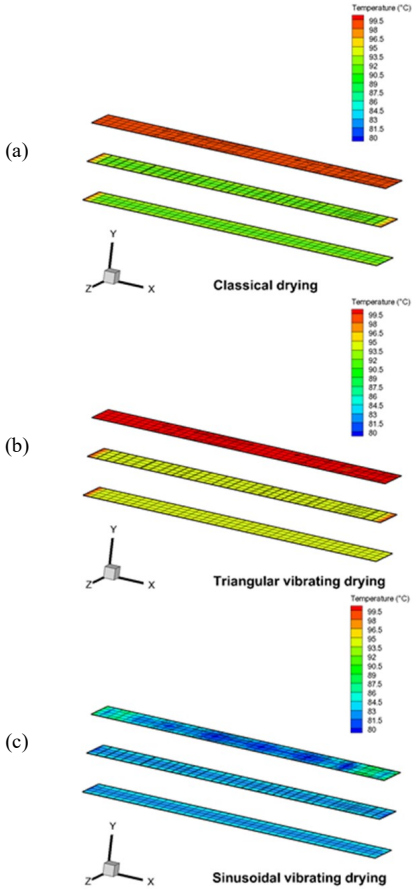

Fig. 9. Comparison of the temperature distribution the during drying process (time=2h) for (a) classical, (b) triangular, (c) sinusoidal drying

The presence of three orthogonal exchange faces forces the moisture content to be very low at the corner. During drying time, only the core of porous plate retains a high value of moisture content (classical drying) (Figure 10). Referring to the result presented in Figure 10, the sinusoidal vibrating mode of drying retains the highest amount of water in the core of the porous medium. As a result, it presents the lowest gaseous pressure compared to the other cases.

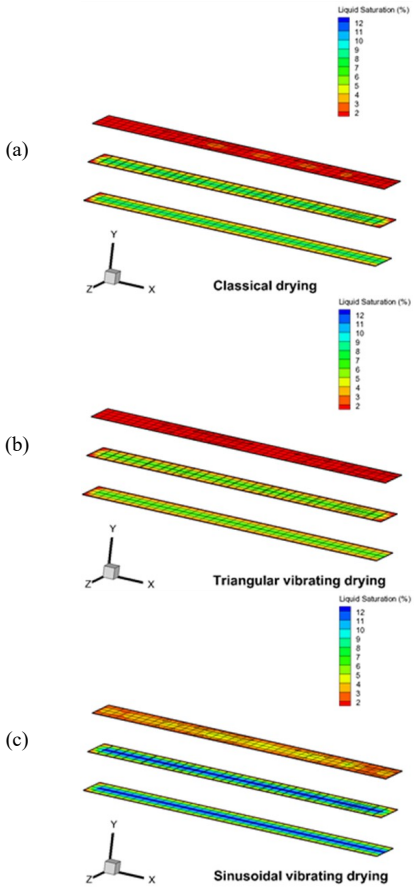

Fig. 10. Comparison of the saturation distribution during the drying process (time=2h) for (a) classical, (b) triangular, (c) sinusoidal drying

Moreover, for the triangular vibration case the liquid water extraction from the core of the porous plate is accelerated, and then dried more rapidly at the exchanging faces. Consequently, the gas pressure in the core of the porous medium is intense forcing the water to migrate to the exchanging faces (Figure 11). From the presented results (Figures 9-11), we can conclude that the drying process becomes more rapid and intense with the triangular vibration which forces the liquid inside the porous plate to migrate to the exchanging faces in order to be dried more rapidly than the two other modes of drying.

VI. CONCLUSIONS

In the present study, a 3-D numerical simulation has been developed to analyze the heat and mass transfer mechanisms that arise during vibrating drying. In order to quantify these effects, two types of external vibration of hot air are tested: triangular and sinusoidal vibrations. Consequently, three configurations of drying of unsaturated porous medium (classical drying, triangular and sinusoidal vibrating drying) are studied.

Referring to the numerical results, these two modes of vibration are characterized by two effects which are totally inverse: the triangular vibrating drying is characterized by a rapid and intense evolution during the drying process, while the sinusoidal vibration leads to slow and weak drying rate. This behavior can be explained by the fact that the resultant heat and mass transfer coefficients take more time to reach their maximum during the sinusoidal vibration and they remain low for a longer time during the vibration period.

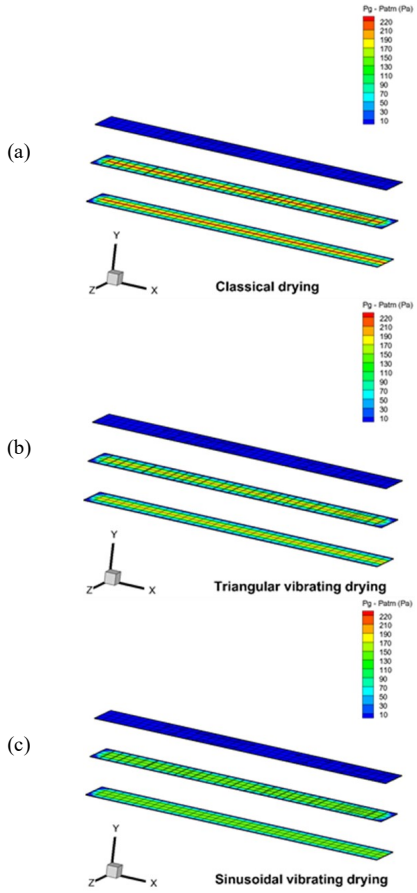

Fig. 11. Comparison of the pressure distribution during the drying process (time=2h) for for (a) classical, (b) triangular, (c) sinusoidal drying

ACKNOWLEDGEMENT

The authors would like to thank the Deanship of the Scientific Research of the University of Hail, Saudi Arabia for funding and supporting the research project (Grant N°0160823).

NOMENCLATURE

a	Acceleration of hot air $[ms^{-2}]$
A_v	Maximum amplitude of hot air velocity $[ms^{-1}]$
C_a	Specific heat of the air $[kJkg^{-1}K^{-1}]$
C_p	Specific heat at constant pressure $[kJkg^{-1}K^{-1}]$
C_v	Specific heat of the vapor $[kJkg^{-1}K^{-1}]$
$D_{A,B}$	Diffusion coefficient $[m^2s^{-1}]$
f_v	Vibration frequency [Hz]
g	Gravitational acceleration $[ms^{-2}]$

h_m Convective mass transfer coefficient $[ms^{-1}]$
h_t Convective heat transfer coefficient$[wm^{-2}℃^{-1}]$
K Intrinsic permeability [m²]
L_c Characteristic length of plate [m]
M_a Molar mass of air $[kgmol^{-1}]$
M_v Molar mass of vapor $[kgmol^{-1}]$
$\dot{m}$ Evaporation rate $[kgs^{-1}]$
n_i Outward normal vector
P Pressure [Pa]
Pc Capillary pressure [Pa]
P_{Vs} Partial pressure of saturated vapor [Pa]
R Gas constant $[Jmol^{-1}K^{-1}]$
r The average radius of curvature of the menisci
S Liquid saturation [%]
T Temperature [K]
T_v Vibration period [s]
t Time [s]
V_a Air velocity $[ms^{-1}]$

Greek symbols
ε Porosity
ε_l Volume fraction of liquid phase
μ Dynamic viscosity $[kgm^{-1}s^{-1}]$
ϑ Kinematic viscosity $[m^2s^{-1}]$
ρ Density $[kgm^{-3}]$
λ Conductive transfer coefficient $[wm^{-1}℃^{-1}]$
σ Surface tension $[Nm^{-1}]$
ΔH_{vap} Vaporisation latent heat $[Jkg^{-1}]$

Subscripts
0 initial condition
a air
eff effective
g gas
l liquid
v vapour

Dimensionless groups
Re Reynolds number
Pr Prandtl number
Sc Schmidt number

REFERENCES

[1] G. Musielak, D. Mierzwa, J. Kroehnke, "Mechanisms of drying acceleration by ultrasounds", 19th International Drying Symposium, Lyon, France, August 24–27, 2014

[2] V. Acosta, J. Bon, E. Riera, A. Pinto, "Ultrasonic drying processing chamber", Physics Procedia, Vol. 70, pp. 854-857, 2015

[3] S. J. Kowalski, "Ultrasound in wet materials subjected to drying: A modelling study", International Journal of Heat and Mass Transfer, Vol. 84, pp. 998-1007, 2015

[4] J. Kroehnke, J. Szadzińska, E. Radziejewska-Kubzdela, R. Biegańska-Marecik, G. Musielak, "Ultrasound- and microwave-assisted convective drying of carrots: Process kinetics and product's quality analysis", Ultrasonics Sonochemistry, Vol. 48, pp. 249-258, 2018

[5] S. M. Beck, H. Sabarez, V. Gaukel, K. Knoerzer, "Enhancement of convective drying by application of airborne ultrasound: A response surface approach", Ultrasonics Sonochemistry, Vol. 21, pp. 2144-2150, 2014

[6] J. Colin, W. Chen, J. Casalinho, M. E. A. Ben Amara, S. Ben Nasrallah, M. Stambouli, P. Perre, "Drying intensification by vibration: fundamental study of liquid water inside a pore", 21thInternational Drying Symposium, Valencia, Spain, September 11-14, 2018

[7] E. A. Kolchanova, N. V. Kolchanov, "Vibration effect on the onset of thermal convection in an inhomogeneous porous layer underlying a fluid layer", International Journal of Heat and Mass Transfer, Vol. 106, pp. 47-60, 2017

[8] E. H. Zidi, A. Hasseine, N. Moummi, "The effect of vertical vibrations on heat and mass transfers through natural convection in partially porous cavity", Arabian Journal for Science and Engineering, Vol. 43, pp. 2195-2204, 2018

[9] R. Rzig, N. Ben Khedher, S. Ben Nasrallah, "A 3-D numerical heat and mass transfer model for simulating the vibration effects on drying process", Heat Transer Asian Research, Vol. 46, pp. 1204-1221, 2017

[10] A. V. Luikov, "Systems of differential equations of heat and mass transfer in capillary porous bodies (review)", International Journal of Heat and Mass Transfer, Vol. 18, No. 1, pp. 1–14, 1975

[11] S. Whitaker, "A theory of drying", Advances in Heat Transfer, Vol. 13, pp. 119-203, 1977

[12] N. Ben Khedher, "Numerical study of the thermal behavior of a composite phase change material (PCM) room", Engineering, Technology & Applied Science Research, Vol. 8, No. 22, pp. 2663-2667, 2018

[13] R. Rzig, N. Ben Khedher, S. Ben Nasrallah, "Three-dimensional simulation of mass and heat transfer in drying unsaturated porous medium", Heat Transfer Research, Vol. 48, No. 11, pp. 985-1005, 2017

[14] A. Latreche, M. Djezzar, "Numerical study of natural convective heat and mass transfer in an inclined porous media", Engineering, Technology & Applied Science Research, Vol. 8, No. 4, pp. 3223-3227, 2018

[15] B. R. Balliga, S. V. Patankar, "A new finite-element formulation for convection–diffusion problems", Numerical Heat Transfer, Vol. 3, No. 4, pp. 393-409, 1980

[16] B. R. Balliga, S. V. Patankar, "A control-volume finite element method for two-dimensional fluid flow and heat transfer", Numerical Heat Transfer, Vol. 6, No. 3, pp. 245–261, 1983

[17] C. Geuzaine, J. F. Remacle, "Gmsh: A 3-D finite element mesh generator with built-in pre- and post-processing facilities", International Journal for Numerical Methods in Engineering, Vol. 79, No. 11, pp. 1309–1331, 2009

[18] F. P. Incropera, D. P. De Witt, T. L. Bergman, A. S. Lavine, Fundamentals of heat and mass transfer, John Wiley & Sons, 2002